

1 Uncertain Effects of DFT Functionals on Time-of-flight
2 Calculations of Organic semiconductor

3 authors

4 September 17, 2024

5 **Abstract**

6 In this paper, the time-of-flight (ToF) is used to quantify the charge mobility in
7 OSC. Using ToF as the quantity of interest, the uncertainty effect of the DFT functionals
8 on the ToF in a BCP device is studied. Using a total of 10 different DFT functionals,
9 we find that the electronic structure properties have similar distributions
10 as indicated by Wasserstein distance, while the ToF can have a relatively large deviation.
11 Further investigation reveals that ToF can be sensitive to the energy of a single
12 molecule, leading to the ToF being sensitive to DFT functionals.

13 Further investigation reveals that the BHANDHLYP functional leads to a trap site,
14 and the charge mobility is very sensitive to the trap sites' energy, so a small change
15 in the site's energy results in a large deviation of ToF. We further estimate the charge
16 mobility distribution due to the uncertainty in electronic structure properties, and
17 those properties' uncertainty is obtained from the maximum likelihood estimation of
18 the 10 data points calculated using the 10 DFT functionals. Ultimately, a confidence
19 level of charge mobility is obtained, and it is found that the uncertainty in site energy
20 has the most significant effect on the ToF.

21 **1 Introduction**

22 Random walks in random environments (RWRE) are widely used to model physical pro-
23 cesses, incorporating the varying levels of disorder and environmental factors that influence
24 movement. These disorders and environmental factors can introduce a level of uncertainty
25 that significantly impacts the overall rates of the random walk, ultimately affecting the
26 quantities of interest one aims to obtain.

27 A notable example of RWRE is charge transport in organic semiconductors (OSCs),
28 characterized by an amorphous mesoscopic structure due to spatially disordered molecular
29 arrangements. This structural disorder translates into electronic structure disorder, including
30 energy disorder and coupling element disorder, leading to the modeling of charge transport
31 processes as continuous time random walks (CTRWs) on a graph. Specifically, the molecules
32 can be represented as nodes in a graph, the transition rates between them (edge weights)
33 correspond to the transition rates between the molecules, and the charge carriers become
34 the random walkers. The details of specifying the graph will be introduced in the Section 2.

35 The uncertainty from electronic structure disorder and environmental factors is reflected in
36 these transition rates.

37 While the transition rates in those CTRWs can be calculated in a first-principle multiscale
38 approach, but it involves some level of approximations. Since the charge transport in OSC
39 involves electrons, quantum mechanics and Schrödinger equation are essential in providing
40 a time-series behavior of the charge dynamics. But due to the complexity of Schrödinger
41 Equation, one alternative theory is the density functional theory (DFT). DFT faces two
42 main challenges: it is computationally impractical for entire OSC devices and the exchange-
43 correlation potential lacks an explicit formula.

44 The first challenge is mitigated by approximating electron dynamics as transition pro-
45 cesses between localized states which contain most of the molecular electron, with transition
46 rates calculated using the temperature-activated bi-molecular Marcus rate. The second chal-
47 lenge is addressed by employing DFT functionals to approximate the exchange-correlation
48 potential. Despite benchmark results on molecular energy calculations with various DFT
49 functionals and extensive literature on charge transport in multiscale models of OSCs, there
50 is a lack of quantitative studies on how DFT functionals affect charge transport processes,
51 and the influence of uncertainty in electronic structure properties.

52 Several challenges arise in this investigation. The high dimensionality of CTRWs (due
53 to the large number of molecules, typically around 1000) makes uncertainty quantification
54 numerically challenging. Secondly, simulating CTRWs is also computationally demanding
55 due to convergence issues. Additionally, the exact DFT exchange-correlation functional and
56 the distribution of transition rates for specific molecules are unknown.

57 One of the main quantities of interest to characterize the charge transport in OSC is
58 charge mobility. Using this as the quantity of interest, the goal of this work is to investigate
59 how the DFT functionals affect the electronic structures and charge mobility. The uncer-
60 tainty due to the environmental factors that cause a change in the molecules' position is not
61 considered in this work, although this topic deserves intensive studies. We want to focus on
62 the following questions:

- 63 • How do DFT functionals change the reorganization energy, distribution of molecule
64 energies and coupling elements?
- 65 • How do DFT functionals change the charge mobility?
- 66 • Which electronic structure (among energy, coupling element and reorganization energy)
67 has the most impact on the uncertainty of charge mobility?
- 68 • Can we estimate the range of the quantity of interest, given a confidence level?

69 Charge mobility, in the presence of an external electric field, can be calculated as $\mu = \frac{\vec{v} \cdot \vec{F}}{|\vec{F}|^2}$,
70 where \vec{v} is the average drift-diffusive velocity of the charge carrier(s). Without an electric
71 field, \vec{v} is the purely diffusive velocity. In electronic devices, velocity is obtained from time-
72 of-flight (ToF) experiments, where charge carriers are injected into the cathode and collected
73 at the anode. The ToF, denoted as τ , is the period from injection to detection of at least
74 one charge carrier. The velocity is given by $|\vec{v}| = \frac{L}{\tau}$, where L is the sample length, usually
75 aligned with the electric field direction if present.

76 For multiscale modeled OSCs, ToF calculations involve setting some molecules as *Source*
 77 and some as *Sink*. The key quantity for characterizing charge transport, especially for
 78 uncertainty quantification, is ToF, as the sample length L is fixed and constant.

79 Most literature on charge transport in multiscale modeled OSCs reports steady-state
 80 charge mobility, using periodic boundary conditions to simulate CTRWs on an infinitely
 81 repeating molecular graph, typically via kinetic Monte Carlo simulations. However, this
 82 method faces challenges, particularly convergence issues, which complicate the accurate cal-
 83 culation of quantities with a desired confidence level.

84 Therefore, this work focuses on characterizing charge mobility based on ToF, specifically
 85 diffusive ToF with a single charge carrier, calculated from the hitting time of a continuous
 86 time Markov chain. This approach excludes the effects of external electric fields, clarifying
 87 the sensitivity from DFT functional to electronic structures and ToF mobility. Furthermore,
 88 considering only one charge carrier aligns with the low carrier density in electronic devices
 89 and avoids the computational complexity of simulating multiple charge carriers, which can
 90 obscure important low-energy molecules in uncertainty quantification.

91 2 Multiscale Model

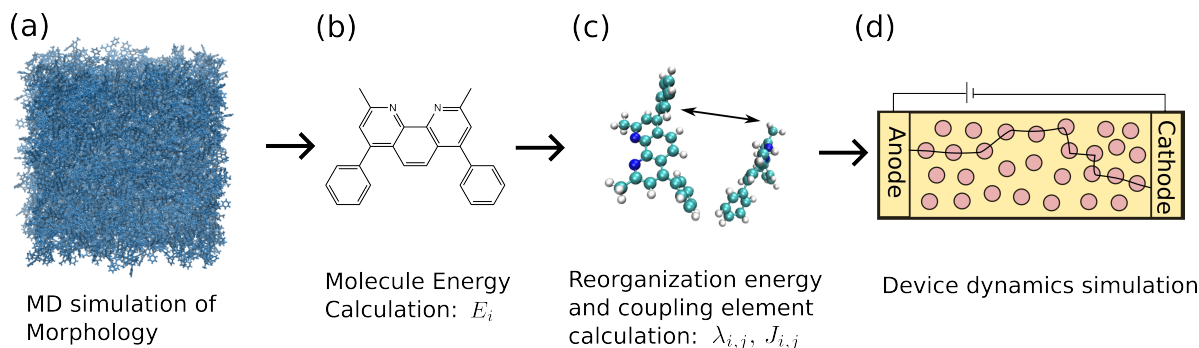


Figure 1: The multiscale model workflow for OSC. Step 1: MD simulation to generate atom coordinates. Step 2: Molecule energy E_i calculation. Step 3: Calculation of Reorganization energy $\lambda_{i,j}$ and coupling element $J_{i,j}$ for pairs of molecule i, j whose COM distance is less than r_{cutoff} . Step 4: Modelling dynamics on device level, such as ToF calculation.

92 Figure ?? shows the workflow of the multiscale model for ToF calculation. In brief
 93 summary, the process includes: Firstly, classical Molecular Dynamics is used to generate the
 94 atomistic coordinates from which the vertex and edge sets are defined. Specifically, using a
 95 cutoff distance r_{cutoff} , any two molecules whose center of mass (COM) within $r_{\text{cutoff}} = 0.5$ [nm]
 96 form a pair of molecules where directed edge weight can be calculated. Secondly, quantum
 97 electronic structure calculation is performed to obtain the electronic structure properties:
 98 The molecule energy E_i of molecule i , the reorganization energy between $\{\lambda_{i,j}\}$ and coupling
 99 element $\{\Delta J_{i,j}\}$ between the pair of molecules i and j . All in unit of eV.

100 Then, those electronic structure properties are used to calculate the bi-molecular Marcus

101 rate between the molecules:

$$\omega_{ij} = \frac{2\pi}{\hbar} \frac{|J_{i,j}|^2}{\sqrt{4\pi\lambda_{i,j}k_B T}} \exp\left(-\frac{(\Delta E_{i,j} + q\vec{F} \cdot \vec{r}_{i,j} - \lambda_{i,j})^2}{4\lambda_{i,j}k_B T}\right), \quad (1)$$

102 where \hbar is the reduced Planck constant, k_B the Boltzmann constant. The temperature T
103 (in K), external electric field \vec{F} and the charge of the carrier q (in e) can be considered as
104 parameters of the simulation. The vector $\vec{r}_{i,j} = (r_{ij}^x, r_{ij}^y, r_{ij}^z)^T$ connects the center-of-masses
105 of molecules i and j , which is calculated using cyclic boundary conditions depending on
106 system setting. And $\Delta E_{i,j} = E_i - E_j$ is the energy difference between a pair of molecules.
107 Finally, the quantity of interest, such as ToF τ , can be calculated from the transition rates
108 ω_{ij} .

109 2.1 Molecule Dynamics Simulation

110 In a material system of N_a atoms with mass and position denoted by m_i and \vec{r}_i respectively,
111 molecular dynamics (MD) models the evolution of the atomic coordinate using Newton's
112 second law, which is written in Hamilton equation:

$$\begin{cases} \frac{d\vec{r}_i}{dt} = \frac{\partial H}{\partial \vec{p}_i} \\ \frac{d\vec{p}_i}{dt} = -\frac{\partial H}{\partial \vec{r}_i} \end{cases} \quad (2)$$

113 for $i = 1, \dots, N_a$, where the Hamiltonian H reads:

$$H = \sum_i \frac{|\vec{p}_i|^2}{2m_i} + U(\vec{r}_1, \dots, \vec{r}_{N_a}) \quad (3)$$

114 In principle the potential energy function $U(\vec{r}_1, \dots, \vec{r}_{N_a})$ of the system can be obtained
115 from electronic structure models. In practice, it is a very computationally expensive proce-
116 dure, and without too much loss in precision, MD use empirical potentials that are designed
117 for specific purposes. In our work, constant the molecule number $N = 1000$, a temperature
118 $T = 300$ K and a pressure at 1 atm is used to achieve an NPT ensemble. One of the final
119 BCP morphology is chosen as OSC for charge transport study.

120 2.2 Electronic Structure Calculation

121 The molecule energy E_i in the multiscale model is calculated as:

$$E_i = (U_i^{cC} - U_i^{nN}) + (E_i^c - E_i^n) \quad (4)$$

122 where U_i^{cC} is the internal energy of charged molecule i in the optimized charged geometry,
123 and U_i^{nN} is the internal energy of neutral molecule i in the optimized neutral geometry. The
124 calculation of U and how to obtain optimized geometry will be introduced in the subsection
125 DFT Calculation. In the superscript the lowercase letter "c/n" represents the molecule
126 state of being charged/neutral and uppercase letter "C/N" represents the geometry of the
127 charged/neutral molecule. This notation also applies for E_i^c , E_i^n . And $E_i^n = E_i^{n,el} + E_i^{n,induce}$

¹²⁸ is the energy due to the electrostatic and induced dipole moment effect. Compared with the
¹²⁹ electrostatic energy calculated using the dielectric constant, this energy in multiscale model
¹³⁰ is very sensitive to the molecule structure, making the uncertainty quantification of charge
¹³¹ transport in multiscale model much more important. A precise method for calculating E_i^n is
¹³² to use the Thole Model as detailed in [1].

¹³³ This method has the steps include: first, each atom a_i is initialized with charges q_{a_i} and
¹³⁴ dipole moment D_{a_i} . Then the induced dipoles of each atom are calculated using the electric
¹³⁵ field generated by other atoms b_j . This calculation continuous iteratively to update the
¹³⁶ induced dipoles of every atom by considering the fields due to other dipoles. Finally, it checks
¹³⁷ for convergence, if the induced dipoles have not changed significantly from one iteration to
¹³⁸ the next, the iterative process stops. Finally, the electrostatic energy and polarization energy
¹³⁹ using the final set of induced dipoles and atomic charges. So in summary, E_i^n is a function
¹⁴⁰ of all atoms' charges and induced dipoles: $E_i^n = \sum_{a_i} f(q_{a_i}, D_{a_i})$.

¹⁴¹ The reorganization energy $\lambda_{i,j}$ between molecule i to molecule j is given as:

$$\lambda_{ij} = U_i^{\text{nC}} - U_i^{\text{nN}} + U_j^{\text{cN}} - U_j^{\text{cC}} \quad (5)$$

¹⁴² The coupling element $J_{i,j}$ between molecule i and j is calculated [2] using the electron
¹⁴³ wave function of the molecules obtained from the Kohn-Sham equation:

$$J_{i,j} = \frac{J_{i,j}^0 - \frac{1}{2}(e_i + e_j)S_{i,j}}{1 - S_{i,j}^2} \quad (6)$$

¹⁴⁴ where $J_{i,j}^0 = \langle \psi^i | \hat{H} | \psi^j \rangle$, $e_i = \langle \psi^i | \hat{H} | \psi^i \rangle$, $e_j = \langle \psi^j | \hat{H} | \psi^j \rangle$, and $S_{i,j} = \langle \psi^i | \psi^j \rangle$ with bra-ket
¹⁴⁵ notation, \hat{H} is the Hamiltonian of the electron wave function, and $\psi^{i,(j)}$ is the electron wave
¹⁴⁶ function of molecule $i(j)$. A single molecule is called a monomer, and a pair of two molecules
¹⁴⁷ is called a dimer.

¹⁴⁸ Denote ψ^D as the electron wave function of the two molecules, $J_{i,j}^0$ can be calculated
¹⁴⁹ via: $J_{i,j}^0 = \gamma^i \text{diag}(\mathcal{E}) \gamma^j$, where $\gamma^i = \langle \psi^i | \psi^D \rangle$ and $\gamma^j = \langle \psi^j | \psi^D \rangle$ are called the projections of
¹⁵⁰ the monomer orbitals ψ^i, ψ^j on the dimer orbitals ψ^D . And $\text{diag}(\mathcal{E})$ is the diagonal matrix
¹⁵¹ consisting of energy eigenvalues of the one-particle wave function of the dimer.

¹⁵² In conclusion, the calculation of electronic structure relies on the internal energy and
¹⁵³ electron wave function. As mentioned in the introduction, DFT is used to calculate these
¹⁵⁴ two quantities. The next subsection will introduce the details of DFT.

¹⁵⁵ 2.3 DFT Calculation

¹⁵⁶ In multiscale model, each molecule is an N_{el} -electron system, and the probability of finding
¹⁵⁷ electrons in space is described by the wavefunction. In DFT, the internal energy calculated
¹⁵⁸ from the Kohn-Sham equation [3] reads:

$$U^{\text{KS}}[\rho] = T_s[\rho] + \int \hat{V}_{\text{ext}}(\vec{r})\rho(\vec{r})d\vec{r} + \hat{V}_{\text{H}}[\rho] + \hat{V}_{\text{XC}}[\rho] \quad (7)$$

¹⁵⁹ where the electron density is $\rho = \sum_{i=1}^{N_{\text{el}}} \phi_i^*(\vec{r})\phi_i(\vec{r})$, $T_s[\rho]$ is the kinetic energy depending on ρ ,
¹⁶⁰ \hat{V}_{ext} is the external potential energy, $\hat{V}_{\text{H}}[\rho]$ is the Hartree energy accounting for the Coulomb

¹⁶¹ interaction, $\hat{V}_{\text{XC}}[\rho]$ is the exchange-correlation energy accounting for the difference between
¹⁶² classical and quantum effect. The exact form of $\hat{V}_{\text{XC}}[\rho]$ is not known, in practice, this energy
¹⁶³ term is approximated by DFT functionals. In our work, ten DFT functionals are used to
¹⁶⁴ represent this energy term. The single-electron wave function ϕ_i satisfies:

$$(-\frac{1}{2}\nabla_{\vec{r}}^2 + \hat{V}_{\text{ext}} + \frac{\delta\hat{V}_{\text{H}}[\rho]}{\delta\rho} + \frac{\hat{V}_{\text{XC}}[\rho]}{\delta\rho})\phi_i^{\text{KS}}(\vec{r}) = \epsilon_i^{\text{KS}}[\rho]\phi_i^{\text{KS}}(\vec{r}) \quad (8)$$

¹⁶⁵ with $\epsilon_i^{\text{KS}}[\rho]$ being the energy eigenvalue of electron i . In practice, Equation 8 is solved
¹⁶⁶ iteratively, and the wave function is represented by a linear combination of basis functions
¹⁶⁷ call basic sets. In this work, the basic set def2-tzvp [4] is used. The DFT computation is
¹⁶⁸ performed by VOTCA [1] which internally calls ORCA software. The internal energy U^{KS}
¹⁶⁹ depends on the atomic coordinates of the molecule. The optimized geometry of a molecule
¹⁷⁰ refers to the atomic coordinates that minimize U^{KS} .

¹⁷¹ 3 Time-of-flight Calculation

¹⁷² The multiscale model defines a graph \mathbf{G} with an adjacency matrix \mathbf{W} , where the edge
¹⁷³ weights $\omega_{i,j}$ represent the Marcus rate from molecule i to molecule j . The charge dynamics
¹⁷⁴ are modeled as a continuous-time random walk on this graph. In the time-of-flight (ToF)
¹⁷⁵ model, some vertices serve as *Source* nodes, representing the electrode where charge carriers
¹⁷⁶ are injected, and some as *Sink* nodes, where charge carriers are detected and the ToF is
¹⁷⁷ recorded.

¹⁷⁸ As mentioned in the introduction, a quantity of interest in modeling charge dynamics is
¹⁷⁹ the ToF, which is the time for charges carriers injected into the Source to be detected at
¹⁸⁰ the Sink. A typical method to obtain the ToF is to use the kinetic Monte Carlo (KMC)
¹⁸¹ method to simulate the CTRW for many times and record ToFs, which are random variables.
¹⁸² To be detailed: But a challenge with this KMC is that one need to repeat a large number
¹⁸³ N_{KMC} of KMC simulation to guarantee an converged ToF. Furthermore, N_{KMC} is not known
¹⁸⁴ before running KMC, posing a great challenge to quantify the uncertainty of ToF from the
¹⁸⁵ multiscale model. An alternative method to overcome the convergence challenge is to obtain
¹⁸⁶ ToF as the hitting time a continuous time Markov chain.

¹⁸⁷ Due to Pauli repulsion, each node can be occupied by at most one charge carrier. For a
¹⁸⁸ system with N molecules and N_c charge carriers, there are $\binom{N}{N_c}$ possible occupation states.
¹⁸⁹ Each occupation state is denoted as \mathbf{s} . A state is called the Source state if all carriers occupy
¹⁹⁰ the Source nodes, and a Sink state if at least one of the Sink nodes is occupied.

¹⁹¹ The transition rates between the states can be obtained from the adjacency matrix \mathbf{W} :
¹⁹² $\omega_{i,j}$, since the connectivity of states is encoded in the connectivity of the nodes, as detailed
¹⁹³ in [5]. According to such connectivity, the transition rates $\Omega_{\mathbf{ss}'}$ from state \mathbf{s} to \mathbf{s}' is:

$$\Omega_{\mathbf{ss}'} = \begin{cases} 0 & \mathbf{s} \text{ is not connected to } \mathbf{s}', \\ \omega_{ij} & \mathbf{s} \text{ is connected to } \mathbf{s}' \text{ due to } (i, j) \end{cases} \quad (9)$$

¹⁹⁴ Then the transition probability from state \mathbf{s} to \mathbf{s}' is $p_{\mathbf{ss}'} = \Omega_{\mathbf{ss}'} / D_{\mathbf{s}}$ where $D_{\mathbf{s}} := \sum_{\mathbf{s}' \neq \mathbf{s}} \Omega_{\mathbf{ss}'}$.

195 And the expected time from state \mathbf{s} to reach the Sink state $\tau_{\mathbf{s}}$ is calculated via:

$$\tau_{\mathbf{s}} = \begin{cases} \frac{1}{D_{\mathbf{s}}} + \sum_{\mathbf{s}' \neq \mathbf{s}} p_{\mathbf{s}\mathbf{s}'} \tau_{\mathbf{s}'} & \text{if } \mathbf{s} \text{ is not a sink state,} \\ 0 & \text{else.} \end{cases} \quad (10)$$

196 To account for all possible starting nodes of the carriers, all Source states must be considered.
197 The random walk process can be modeled as a parallel electric network of capacitors [6].
198 Accordingly, the ToF is evaluated using the harmonic mean:

$$\tau = N_{\text{source}} \left[\sum_{\mathbf{s} \in \text{Source}} (\tau_{\mathbf{s}}^*)^{-1} \right]^{-1}, \quad (11)$$

199 where N_{source} is the number of Source states.

200 4 Results on BCP

201 A OSC device consisting of 1000 BCP molecules arranged in $8 \times 8 \times 8$ cubic box is simulated using MD, as shown in Fig. 1(a). The *Source* contains molecules whose COM have 202 X-coordinates $0 < r_i^x < 0.5$ nm, and *Sink* molecules $7.5 < r_i^x < 8$. This section presents 203 the molecule energy distribution, coupling element distribution, reorganization energies and 204 ToFs calculated using the 12 DFT functionals. Using the PBE0 functional as a reference, 205 the difference in electronic structure distributions due to DFT functionals is measured by the 206 Wasserstein distance. In contrast to the small Wasserstein distance between the electronic 207 structure distributions, the difference in ToF $\Delta\tau$ is relatively large. Next, the change of the 208 graph connectivity due to different DFT functionals is used to explain the $\Delta\tau$. Following 209 this, a normal distribution estimated from maximum likelihood is used to represent the un- 210 certainty in each electronic structure parameters. Then distributions of ToF are obtained 211 using the electronic structure parameters generated by Monte Carlo sampling from the esti- 212 mated distributions. Finally, the sensitivities of $E_i, J_{i,j}, \lambda_{i,j}$ to ToF are compared, confidence 213 level of ToFs are estimated.
214

215 4.1 Electronic Structure Parameters and ToFs

216 Using ten different functionals, the molecule energies, coupling elements and reorganization 217 energies are calculated from the multiscale model with ten different DFT functional.

218 Table 1 summarizes the names of the DFT functionals, the amount of Hartree-Fock 219 exchange (HFX), the reorganization energies, ToFs, the standard deviation of the molecule 220 energy distributions, the drift ToFs under an electric field 6×10^7 V/m and mobility. The 221 table indicates that while the energy standard deviations $\sigma(E)$ are similar across different 222 functionals, the ToF vary significantly, notably for functionals like BHANDHLYP, M06L, 223 and BHLYP.

224 The functional BHANDHLYP gives a ToF much larger than the rest of the 9 functionals.
225 The reason for this large ToF in BHANDHLYP is that one molecule has relatively low 226 energy, and the out-going rate for this molecule is very small, eventually leading to large

Functional	HFX	$\lambda_{i,j}$ [eV]	ToF [s]	$\sigma(E)$	drift ToF [s]	μ [m/s]
PBE0	0.25	0.388	1.23×10^{-3}	0.175	1.44×10^{-6}	9.40×10^{-7}
PBE	0	0.303	1.04×10^{-3}	0.172	2.27×10^{-7}	5.95×10^{-6}
B3LYP	0.20	0.375	4.28×10^{-3}	0.175	3.22×10^{-7}	4.08×10^{-6}
BHANDHYP	0.5	0.494	737.94	0.192	4.75×10^{-2}	2.86×10^{-11}
TPSS	0	0.310	1.37×10^{-2}	0.168	1.03×10^{-6}	1.30×10^{-7}
BP86	0	0.304	7.46×10^{-3}	0.175	5.81×10^{-7}	2.33×10^{-6}
wB97X	0.157	0.505	2.92×10^{-2}	0.191	2.01×10^{-6}	6.74×10^{-7}
wB97X-D3	0.195	0.496	4.89×10^{-2}	0.180	2.50×10^{-6}	5.42×10^{-7}
M06L	0	0.312	0.319	0.165	2.11×10^{-5}	6.42×10^{-8}
BHLYP	0.5	0.493	2.47	0.192	5.96×10^{-5}	2.28×10^{-8}

Table 1: DFT functional HF exchange scaling (HFX), calculated values of reorganization energy ($\lambda_{i,j}$), diffusive ToF, energy disorder ($\sigma(E)$), drift ToF, and mobility (μ) for BCP molecules for different DFT functionals.

227 ToF. However, such large difference in a material system is non-physical, and studying the
 228 uncertain quantification based on those ToF data can not indicate anything on the robustness
 229 of the multiscale model.

230 A noticeable difference in all the different functional is the amount of HF for approxi-
 231 mating the exchange-correlations.

232 So by fixing the functional to be the commonly used PBE0 functional, the HFX is varied
 233 to investigate the effect of HFX to the molecular properties and ToF. Hybrid functionals like
 234 PBE0 or B3LYP use a specific, empirically determined fraction of HF exchange that generally
 235 works well for a broad range of applications. PBE0 is constructed by combining 25% of the
 236 exact exchange from HF theory with 75% of the exchange from the Perdew-Burke-Ernzerhof
 237 (PBE) GGA exchange functional, along with the full PBE correlation functional.

238 When correlation effects are strong and electron-electron interactions play a significant
 239 role in determining their physical properties, the exact exchange overly localize electrons, and
 240 a lower HFX percentage or even pure DFT might perform better. The π -electron conjugation
 241 and interactions in OSC such as BCP and MADN leads to significant electronic correlation
 242 effects within those materials.

243 4.2 BCP molecule with different HFX

244 So our first investigation use the range of HFX=0.05, 0.15, 0.23, 0.24, 0.25, 0.26, 0.27, 0.35, 0.45, 0.55.
 245 The values of HFX=0.23, 0.24, 0.26, 0.27 are used because we want to see if a small pertur-
 246 bation in HFX would affect ToF significantly.

247 Since ToF is sensitively affected by site energy, which is affected by the isotropic polariz-
 248 ability P_{iso} and dipole moment μ of the molecules, we plot the those molecular properties as
 249 a function of HFX. The Fig.2(a) shows that as HFX increase, the dipole moment increases
 250 first linear in the range of HFX=0.05 to 0.35, then a relatively large increase at HFX=0.35
 251 to 0.55.

252 Figure 2(b) shows that as HFX increase, the n state and h state BCP molecule has
 253 decreasing isotropic polarizability, showing that the molecule is getting more difficult to be

254 polarized. Since the isotropic polarizability is decreasing as HFX increases, the screening
 255 effects are weaker for large HFX.

256 Fig.2(c) shows that as HFX increase, reorganization energies are higher. Since the
 257 molecule requires more energy to reorient itself during the charge transfer process, the higher
 258 reorganization energy can slow down charge transport by making it energetically more costly
 259 for charges to move between molecules.

260 Fig.2(d) shows that when HFX=0.05-0.3 the energy disorder is relatively small (less than
 261 0.2 eV). When HFX=0.35-0.55, the energy disorder $\sigma(E) > 0.22$.

262 The ToF of the BCP molecular system calculated using different HFX is shown in table
 263 2. This table shows that for HFX=0.35,0.45,0.55, the ToFs are extremely large compared
 264 to the ToFs for HFX<0.3. In contrast to the almost linear HFX- λ relationship, those large
 265 ToFs are not physical.

HFX	ToF [s]	ToF(no E) [s]
0.05	0.32010	3.004×10^{-10}
0.15	0.3879	4.668×10^{-10}
0.23	0.0200	6.787×10^{-10}
0.24	0.02977	7.0290×10^{-10}
0.25	0.02648	7.633×10^{-10}
0.26	3.259	7.824×10^{-10}
0.27	0.0359	9.162×10^{-10}
0.35	1.72×10^7	1.00×10^{-9}
0.45	1.8×10^4	1.32×10^{-9}
0.55	1.23×10^9	1.880×10^{-9}

Table 2: The ToF with and without energy disorder of the BCP system as a function of the HFX.

266 The reason for this non-physical ToF is that the site energy calculation use the atomic
 267 charges and molecular polarizability from the optimized BCP structure. However, each
 268 molecule in the BCP system has its own topology with different atomic charges and polar-
 269 izability compared to the optimized BCP structure. Those difference in atomic charges and
 270 polarizability affect the site energy calculations.

271 So the atomic charges and polarizability in the optimized structure can not be transferred
 272 to the BCP molecules generated from the MD simulation. For very disorder material system
 273 such as BCP, using the atomic charges and polarizability in the optimized structure can
 274 result in site energies that are deviated from the majority of the molecules.

275 Figure 3 shows that for HFX<0.3, the site energies of all molecules are relatively close
 276 to the site energy obtained from PBE0 functional. When HFX=0.35, 0.45, 0.55, there are
 277 obvious low-energy molecules. Those low molecules results in the large energy disorder $\sigma(E)$
 278 as shown in table 1. For those three systems the ToFs are extremely large.

279 The site energy has the contribution from the electrostatic effect and polarization effect
 280 due to the dipole moment of the molecules. The Heat map of the electrostatic energy and
 281 polarization energy are shown in Fig.4 and Fig.5.

282 Figure 4 shows that for all HFX parameters, the electrostatic energy are relatively close,
 283 while Fig.5 shows that for HFX=0.35,0.45,0.55, there are molecules that have small polar-

²⁸⁴ ization energy, contributing to the small site energies, and the extremely large ToF. Those
²⁸⁵ small polarization energies and site energies are not physical. When HFX is varied, the
²⁸⁶ change of the polarizability and reorganization energy are almost linear, while there is huge
²⁸⁷ jumps in those site energies due to the huge jumps in the polarization energy.

²⁸⁸ So for correlated system such as OSCs, large range of HFX leads to non-physical results.
²⁸⁹ In the next section, we will use the range with small HFX values for the investigation of a
²⁹⁰ less disorder molecular system, MADN.

²⁹¹ 5 Results on MADN

²⁹² MADN (2-Methyl-9,10-di(naphth-2-yl)anthracene) is another type of OSC. The ToFs with
and without energy disorder for $HFX = 0.0, 0.05, 0.10, 0.15, 0.20, 0.25$ are shown in

HFX	ToF [s]	ToF(no E) [s]
0.00	6.41×10^{-9}	1.88×10^{-10}
0.05	6.37×10^{-9} (estimate)	2.63×10^{-10}
0.10	1.74×10^{-8} (estimate)	3.31×10^{-10}
0.15	3.03×10^{-8}	3.96×10^{-10}
0.20	2.61×10^{-8} (estimate)	7.06×10^{-10}
0.25	9.54×10^{-8}	7.24×10^{-10}

Table 3: The ToF with and without energy disorder of the MADN system as a function of the HFX.

²⁹³

²⁹⁴ References

- ²⁹⁵ [1] Victor Rühle, Alexander Lukyanov, Falk May, Manuel Schrader, Thorsten Vehoff, James Kirkpatrick, Björn Baumeier, and Denis Andrienko. Microscopic simulations of charge transport in disordered organic semiconductors. *Journal of Chemical Theory and Computation*, 7(10):3335–3345, 2011. PMID: 22076120.
- ²⁹⁹ [2] Björn Baumeier, James Kirkpatrick, and Denis Andrienko. Density-functional based determination of intermolecular charge transfer properties for large-scale morphologies. *Physical Chemistry Chemical Physics*, 12(36):11103, 2010.
- ³⁰² [3] W. Kohn and L. J. Sham. Self-Consistent Equations Including Exchange and Correlation Effects. *Physical Review*, 140(4A):A1133–A1138, November 1965.
- ³⁰⁴ [4] Florian Weigend. Accurate Coulomb-fitting basis sets for H to Rn. *Physical Chemistry Chemical Physics*, 8(9):1057, 2006.
- ³⁰⁶ [5] Zhongquan Chen, Pim van der Hoorn, and Björn Baumeier. Graph Random Walk for Time-of-Flight Charge Mobilities, 2024. Version Number: 1.
- ³⁰⁸ [6] Peter G. Doyle and J. Laurie Snell. Random Walks and Electric Networks. 2000. Publisher: arXiv Version Number: 1.

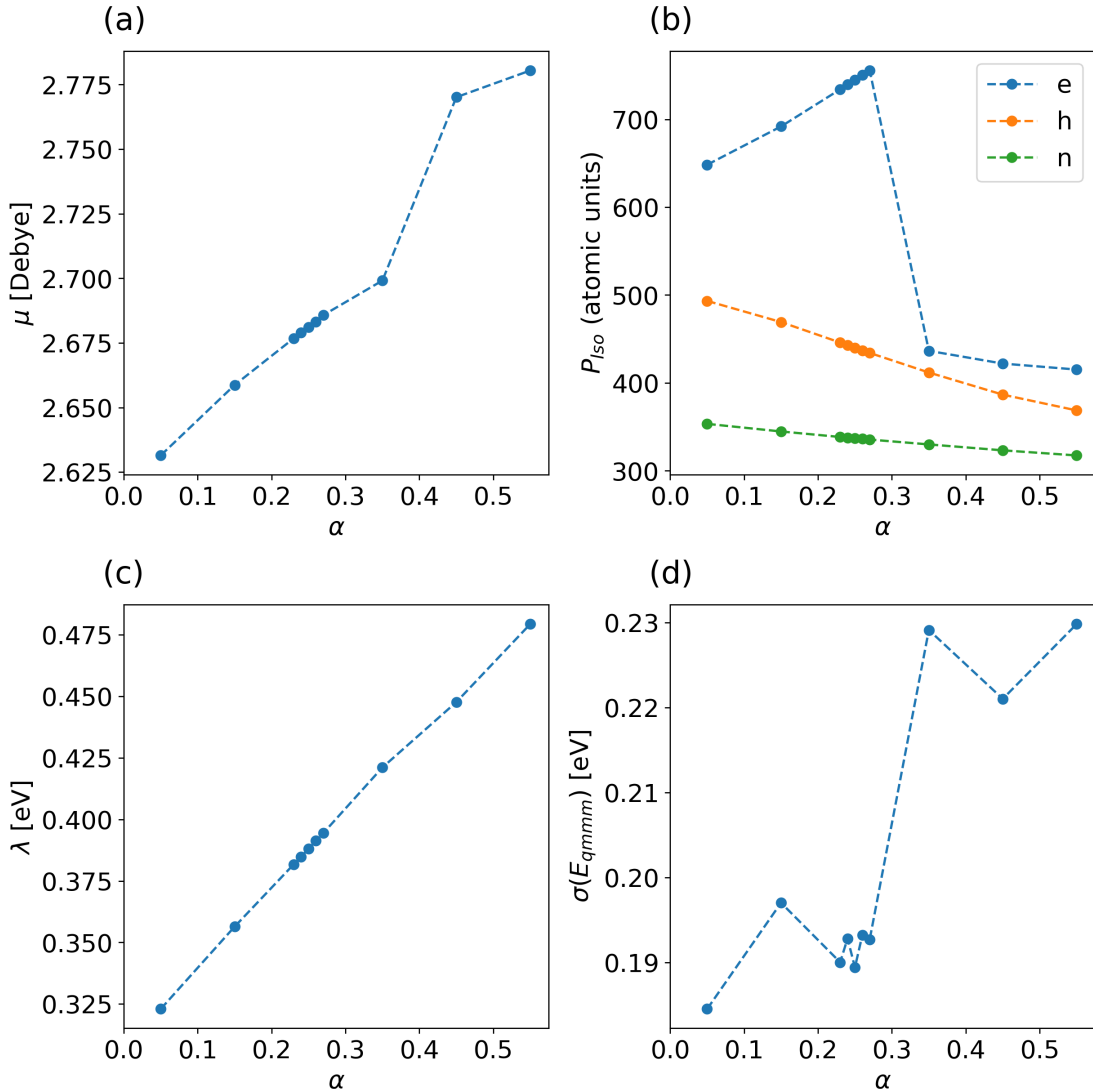


Figure 2: (a) The neutral state BCP molecule dipole moment μ , (b) isotropic polarizability P_{iso} , (c) reorganization energies λ and (d) energy disorder $\sigma(E)$ as a function of the HFX parameters.

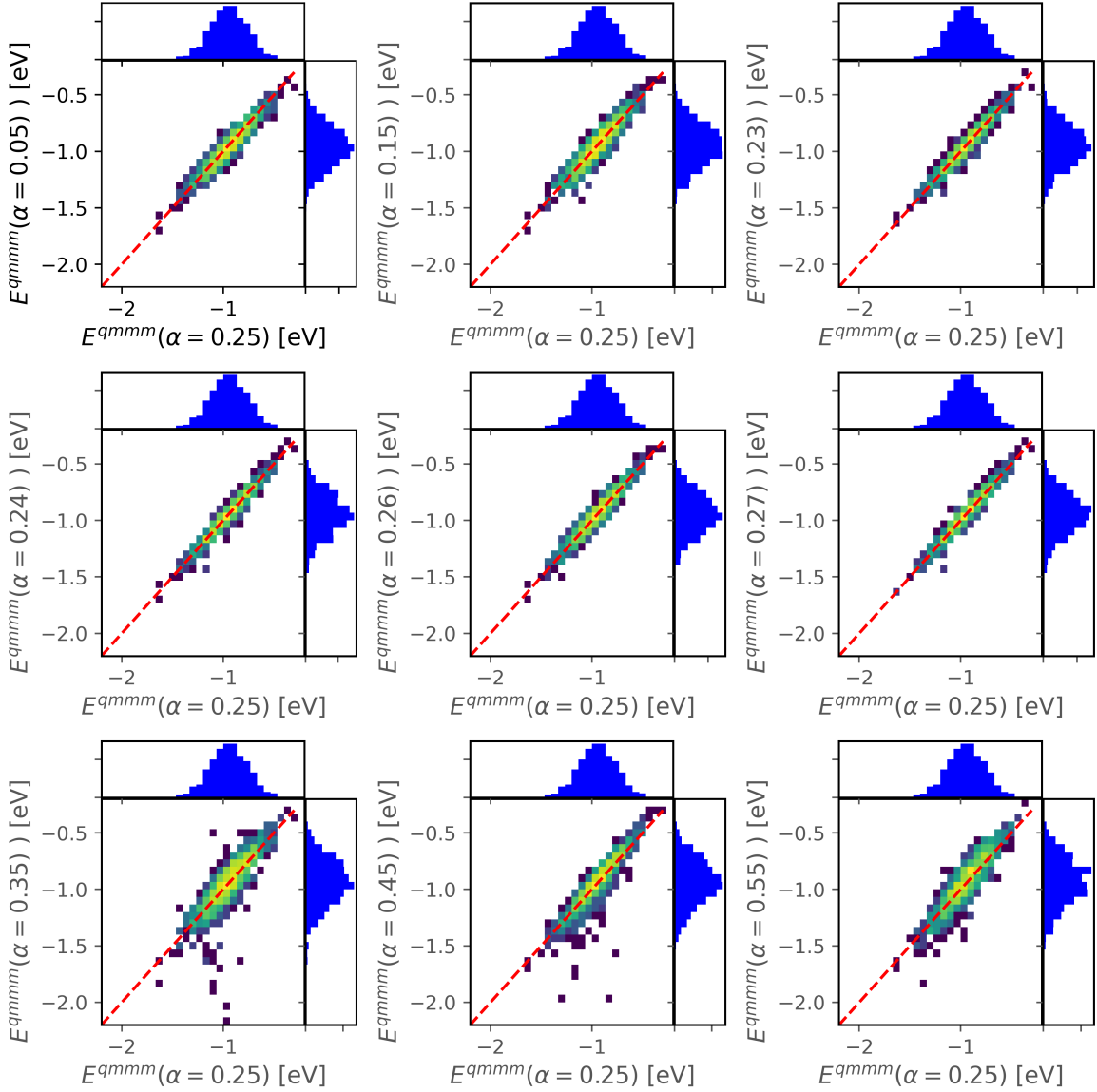


Figure 3: Scatter plot of site energy calculated from different HFX, compared to the site energy calculated from HFX=0.25 (The PBE0 functional). The brighter color near the diagonal lines indicates denser population of the molecules. The top and right histogram show the energy distributions.

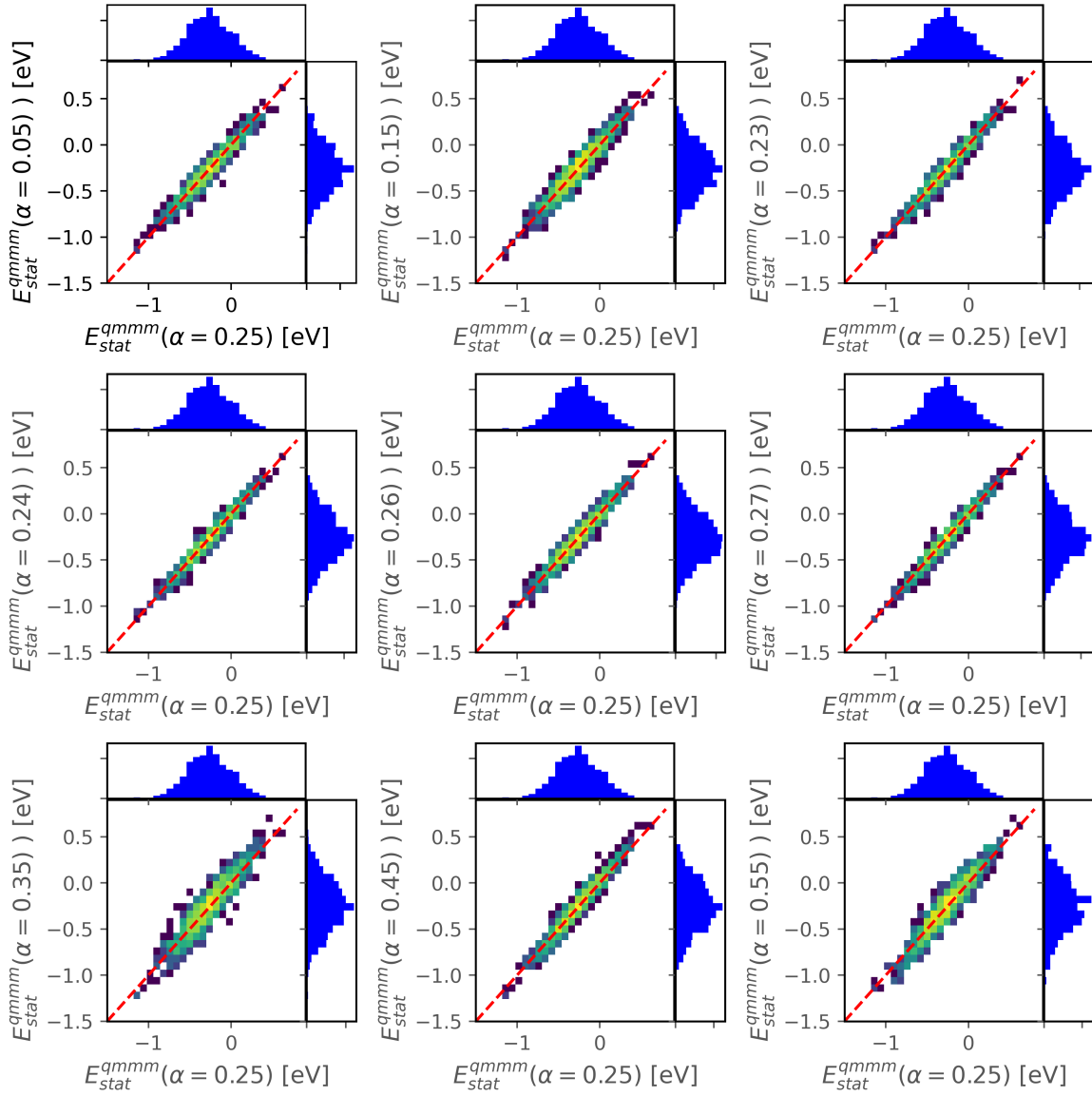


Figure 4: Scatter plot of electrostatic energy calculated from different HFX, compared to the electrostatic energy calculated from HFX=0.25 (The PBE0 functional). The brighter color near the diagonal lines indicates denser population of the molecules. The top and right histogram show the energy distributions.

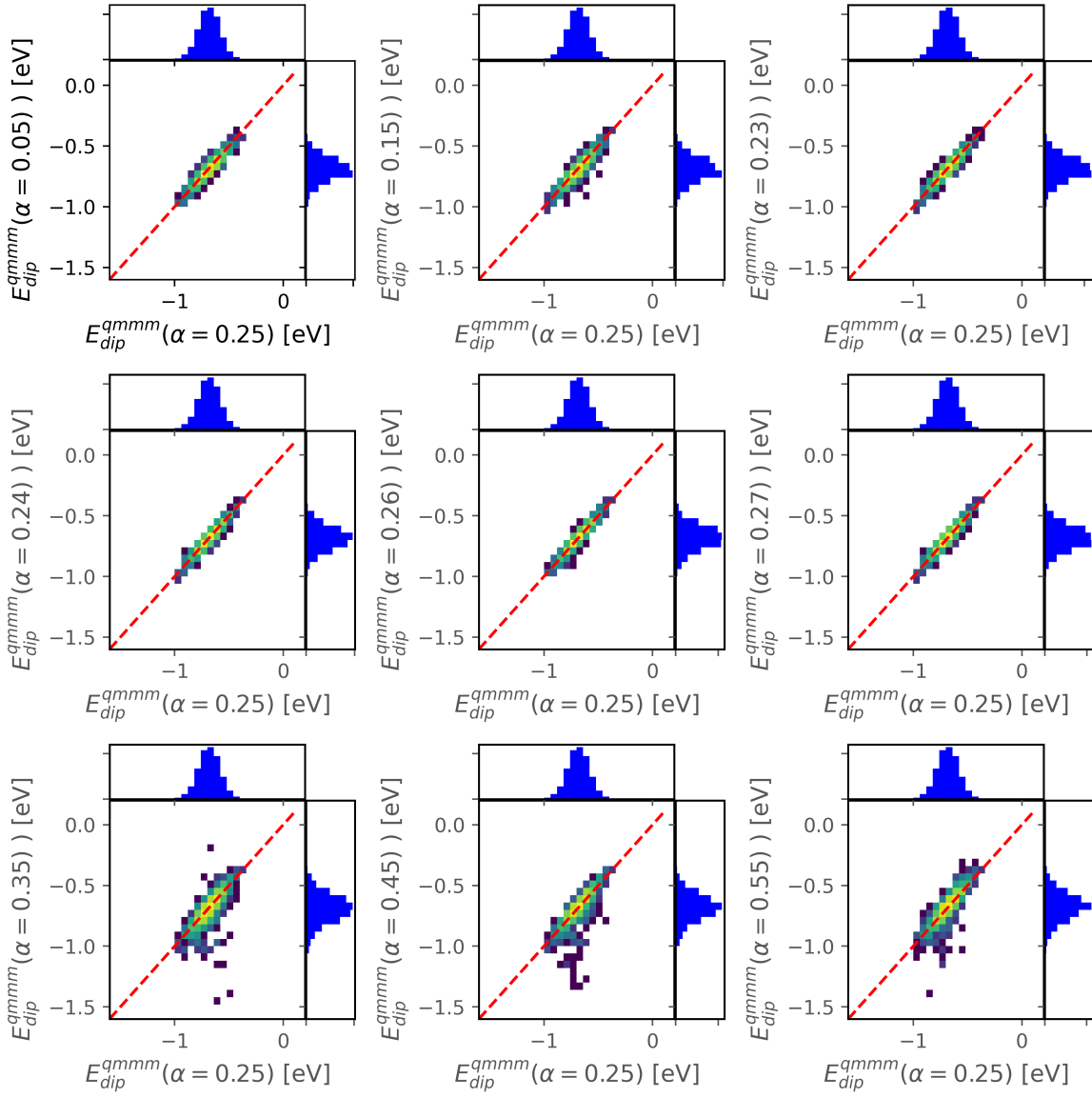


Figure 5: Scatter plot of polarization energy calculated from different HFX, compared to the polarization energy calculated from HFX=0.25 (The PBE0 functional). The brighter color near the diagonal lines indicates denser population of the molecules. The top and right histogram show the energy distributions.